AIMS Materials Science, 6(1): 63–79.
DOI: 10.3934/matersci.2019.1.63
Received: 19 August 2018
Accepted: 18 January 2019
Published: 23 January 2019

http://www.aimspress.com/journal/Materials

Research article

Modelling and analysis of strain hardening characteristics of sintered steel preforms under cold forging

Ananthanarayanan Rajeshkannan[1],*, Sumesh Narayan[2] and A.K. Jeevanantham[3]

[1] Associate Professor, Mechanical Engineering, School of Engineering and Physics, Faculty of Science, Technology & Environment, The University of the South Pacific, Laucala Campus, PO Box 1168, Suva, Fiji
[2] Senior Lecturer, Mechanical Engineering, School of Engineering and Physics, Faculty of Science, Technology & Environment, The University of the South Pacific, Laucala Campus, PO Box 1168, Suva, Fiji
[3] Professor, Department of Manufacturing Engineering, School of Mechanical Engineering, VIT University, Vellore-632014, Tamil Nadu, India

* **Correspondence:** Email: ananthanarayanan_r@usp.ac.fj; Tel: +6793232695; Fax: +6793231538.

Abstract: An attempt has been made to model strain hardening parameters for sintered iron and iron-0.4% carbon steel preforms that are subjected to cold upsetting. The aspect ratios and lubricants are also considered as variables apart from the compositions. The 2^3 factorial design has been considered to design the experiment and subsequently Yate's algorithm is utilized to construct the model. The model has further been refined using analysis of variance. The final model adequacy is determined through correlation coefficient which is predicted to follow near unity. Thus the mathematical model can be utilized to predict strain hardening parameters such as strength coefficient, K, and strain hardening exponent, n, subsequently to design the process parameters to inculcate the required strain hardening characteristics within the range of process parameters specifications that are considered in the present investigation.

Keywords: strength coefficient; strain hardening exponent; factorial design; ANOVA

1. Introduction

Powder metallurgy (P/M) process has several benefits over conventional processes which puts it in the prime position for further research and developments. It was presented elsewhere that the parts produced by P/M process provides reduced specific density, improved corrosion and wear resistance, reduced thermal expansion and high strength to weight ratio [1,2]. It was reported that the P/M process is sustainable as it is able to reduce wastage by near net shape production [3]. Besides the energy consumption can be significantly reduced and is environmentally friendly as it does not produce harmful gases as in liquid state processing of such materials [4]. The conventional P/M process includes powder blending or mixing followed by cold, hot or warm compaction and finally the sintering process. The parts produced through this conventional P/M process inherits substantial amount of pores limiting its industrial use in high strength applications. To make such parts more useful in industry a secondary P/M operation is necessary. In the context of secondary P/M operations, metal deformation particularly cold deformation process takes advantage over powder extrusion, infiltration, heat treatment, etc. This is because the plastic deformation is the main way to improve the density of the P/M materials and ultimately its strength and performance. It was described elsewhere that the preforms produced by primary P/M process will undergo severe plastic deformation during cold deformation due to the presence of substantial amounts of pores [5]. As such, strain hardening is a critical factor in the study of plastic deformation of materials particularly for P/M materials.

Luo et al. described that during plastic deformation of P/M materials, the stress continuously increases as the strain increases to produce continuous slip [6]. This is because the material undergoes strain or work hardening phenomenon and as the pores close during plastic deformation more stress is required for additional plastic deformation. It was presented that the failure of P/M materials that is appearance of visible crack on the surface can be commonly represented by ductile fracture mode [7]. The ductile failure mode depends on strain, stress, strain rate, friction, strain hardening, part geometry, amount of pores, etc. Ebrahimi and Pardis described that the fundamental Ludwick equation can be used to analyse the experimental strain stress curve for P/M materials and two important parameters of this theory are the strength coefficient (K) and strain hardening exponent (n) [8]. It was shown that the value of strength coefficient increases as the strength of the material increases due to plastic deformation which in turn closes the pores in the P/M materials whereas the value of strain hardening exponent is dependent on the plastic deformability of the material [5]. Pore volume decreases during compressive loading causing geometric strain hardening. Bouaziz et al. studied the effects of composition on work hardening characteristics of TWIP steels and presented a model that designers can use to produce Fe-Mn-C alloy with required composition to acquire desired mechanical properties [9]. The weight percentage of carbon in powder metallurgy steels were reported to play a vital role and affected the final products densification and deformation behaviour, strain hardening parameters as well as mechanical properties. It is noted that the strength coefficient, decreased and the strain hardening exponent, increased with increasing carbon particles in the powder metallurgy steels [10].

It was reported elsewhere that the friction plays a critical role during cold upsetting as metal flow, densification, strain hardening and workability depends on it [11]. Lubricants are important as it reduces friction during cold upsetting and problems like high pressure requirement during part ejection, tool wear and poor surface quality can be avoided if correct lubricant is utilized. It was

demonstrated that the lubricants such as zinc stearate, molybdenum disulfide, grease, graphite mixed in acetone are some common lubricants used to reduce between preform and die surfaces [12]. The effect of utilizing different lubricants were studied and reported that grease lubricant showed higher densification and strength coefficient over molybdenum disulfide and graphite lubricants [13]. Further, they reported that the initial preform geometry played a significant role in the influence of densification and strain hardening parameters. Li et al. evaluated the effect of reinforcements and lubricants on the die wear during the cold upsetting process [14]. Apart from many other factors such as compaction load, particle shape and size, lubricant showed significant contribution towards die wear during cold upsetting. Preform geometry also plays a significant role in the establishment of strain hardening characteristics as the amount of pores and its orientation is dependent of preform geometry. The amount of pores and its orientation is critical during cold compaction of P/M parts. The workability, strain and stress behaviour of AISI 9840 and AISI 9845 powder metallurgy steels during cold upsetting were investigated and it was noted that the lower aspect ratio preforms showed better densification and workability characteristics when compared to higher aspect ratio preforms [15].

It was observed from the literature that there is not much effort has been made to model the process parameters for the deformation characteristics of P/M material. In the present investigation, this research gap was taken into account and the attempt has been made to model the process parameters of the strain hardening characteristics of P/M steel preforms under the influence of preform geometry, friction conditions and compositions. The mathematical modelling is expected to determine the strain hardening parameters as close to the experimental prediction, which in turn avoid doing excessive experimental work within the prescribed tolerance of the process parameters considered.

2. Research methodology

The flow chart for the methodology followed in the present investigation is shown in Figure 1. It is evident that the research work initiated from the literature review to study the deformation behaviour of powder metallurgy P/M material and its main influencing process parameters. The main effects and its levels are identified accordingly the design matrix were set up to conduct the experiment. This is followed by delineating the strain hardening characteristics and the prediction of strength coefficient and strain hardening parameter. Finally the model is formulated using Yate's algorithm and ANOVA process ended with residual analysis, before that the model adequacy were checked to find the best fit.

3. Identifying the main effects and its levels

The present research work main effects are considered as the compositions, aspect ratios and friction conditions under which the cold upsetting is carried out. Each main parameter consists of two levels respectively termed as low and high, which is depicted in Table 1.

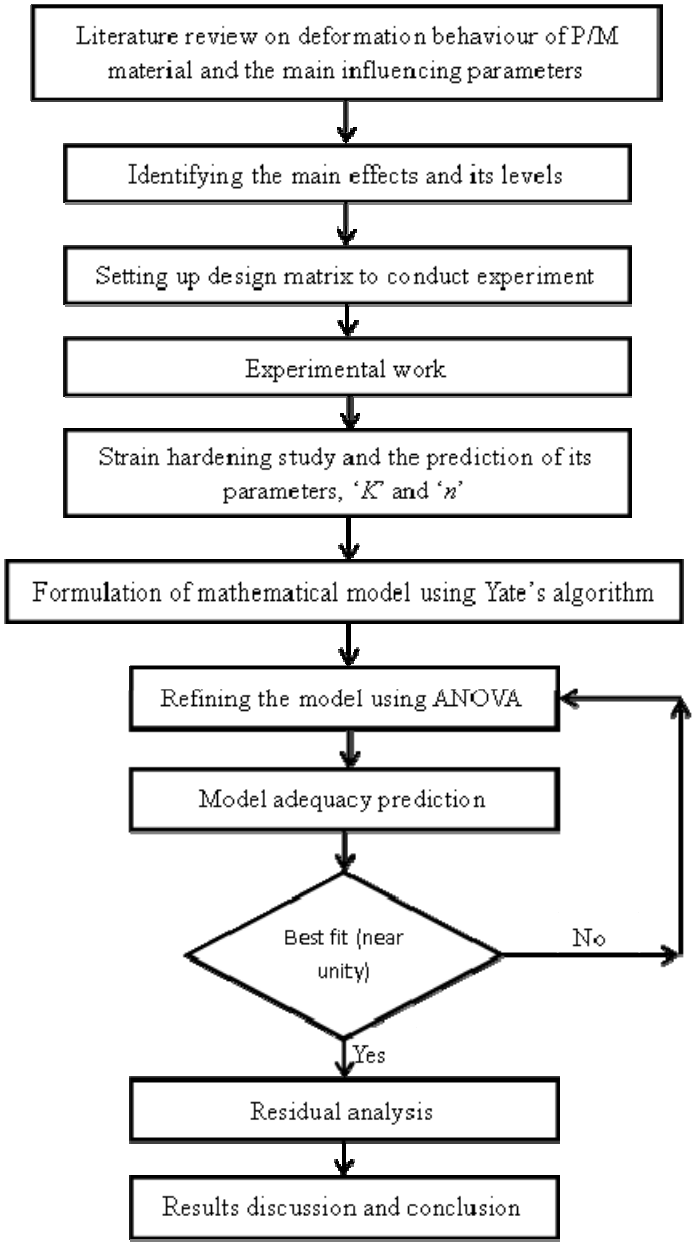

Figure 1. Research methodology.

Table 1. Main effect and their levels.

S. No.	Main effects	Notation	Levels			
			Actual		Code	
			Low	High	Low	High
1	Composition	C	Fe	Fe-0.4%C	−1	1
2	Aspect Ratio	A	0.3	0.6	−1	1
3	Lubricant	L	Dry	Graphite	−1	1

Conventionally, any change of levels within the specification range needs fresh experiment to predict deformation characteristics as a consequence the experimentation includes extra cost, waste

of resource and time consuming. Thus, an attempt has been made to formulate the mathematical model to overcome these challenges in the present work.

4. Design matrix

Table 1 shows three different process parameters and its two actual levels, for both the levels of each variable or main effect the notations as well as the coding value are assigned. Usually for low level −1 and for high level +1 are used. In between the two actual levels, the required coding values shall be determined by the following expression as explained elsewhere [16].

$$C_i = \frac{C_x - [(C_{max} + C_{min})/2]}{[(C_{max} - C_{min})/2]} \quad (1)$$

where C_i is the required coded value of main effect of any value C_x between C_{min} and C_{max}; C_{min} is the lower level of the main effect and C_{max} is the higher level of the main effect.

The coding values are used for the convenience of making the statistical analysis, in addition if the main effect is happened to be the qualitative aspect such as in the present work, compositions, shall be termed quantitatively as a coded value. The 2^3 factorial design has been utilized to design the matrix for the present work in order to include all the possible combinations of levels. The term "3" represents the number of the main effects. Table 2 shows the design matrix, which explains the order of experiment from 1 through 8 with combination of variables for each experiment order.

Table 2. Experimental design matrix with the predicted *K* and *n* values.

Standard order	Coded factors			K in MPa		n	
	C	**A**	**L**	Trial 1	Trial 2	Trial 1	Trial 2
1 or [1]	−1	−1	−1	125	120	0.4	0.41
2 or C	1	−1	−1	120	112	0.41	0.43
3 or A	−1	1	−1	99	90	0.44	0.47
4 or CA	1	1	−1	96	90	0.43	0.44
5 or L	−1	−1	1	91	110	0.46	0.41
6 or CL	1	−1	1	100	99	0.44	0.43
7 or AL	−1	1	1	76	90	0.46	0.45
8 or CAL	1	1	1	87	79	0.46	0.48

Although the design matrix is considered as base to conduct experiment, the experiments were not conducted as per the design matrix instead it was done in random order to avoid the systematic error infiltration. The two different trails of experiments were performed to determine the out variables such as strength coefficient, *K* and strain hardening exponent, *n*. In Table 2, the variable *C*, *A* and *L* are main effects and *CA*, *CL*, *AL* and *CAL* are interaction effects. The standard order "[1]" represents that the experiment carried out using low levels on each variable.

5. Experimental work

Iron and graphite powders of −150 μm and −3 μm respectively are used to prepare Fe and Fe-0.4%C alloy preforms. Cylindrical preforms with the aspect ratios of 0.3 and 0.6 on each composition were prepared. The purity of iron powder was analysed to be 99.7%. The apparent density (AD), flow rate (FR) measured with hall flow meter and compressibility (ρ) at 420 ± 10 MPa of Fe powder and Fe-0.4%C blend are shown in Table 3.

Table 3. Properties of Fe powder and Fe-0.4%C blend.

Si. No.	Property			Fe		Fe-0.4%C				
1.	AD (g/cc)			3.38		3.35				
2.	FR (s/50g)			26.3		28.1				
3.	ρ (g/cc)			6.46		6.26				
4. Sieve size analysis of iron powder										
Sieve size (μm)	150	+126	+106	+90	+75	+63	+53	+45	+37	−37
Wt% retained	9.16	22.62	10.36	1.1	19.14	13.06	10.17	4.77	0.51	7.8

The amount of powders required to prepare Fe-0.4%C blend were taken and homogenously mixed using a ball mill machine. A hydraulic press with a capacity of 100 tons was used to compress this powder blend and a load of 420 ± 10 MPa was required to achieve an initial relative density of 0.86 ± 0.01. The compressed preforms were ceramic coated to prevent contamination and surface reaction with the air due to high temperatures during sintering. Then the preforms were sintered in a furnace at 1120 ± 10 ºC for 90 minutes followed by furnace cooling of the preforms. The cooled sintered preforms were machined to acquire the required height to diameter ratios and were subjected to upsetting operations using a flat die set. The load was varied in the increments of 0.04 MN and each time the following measurements were taken until surface cracks were visible, deformed height, bulged diameter, top surface contact diameter, bottom surface contact diameter and preform density. The open die upsetting experiments were conducted at two different friction settings; one is dry or nil lubricant and the other one is graphite employed lubricant condition. Experimental measurements were used to compute the true stress and true strain to delineate and predict the strain hardening characteristics of the preforms.

6. Strain hardening characteristics and prediction of its parameters

The plot (Figure 2) shows strain hardening behaviour of Fe and Fe-0.4%C with the influence of aspect ratios and lubricants under cold upsetting operation.

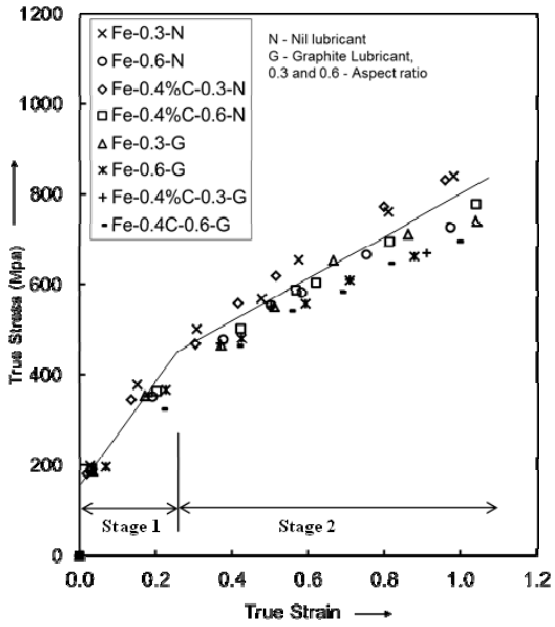

Figure 2. Stress-strain behaviour.

It can be observed in general that inducing the strain proportionally increasing the stress for all the combination of variables; however, raise in stress shows two different stages. The initial stage is relatively shorter span as compared to the second stage that possess maximum span and it is found to be rising gradually. The second stage observed to prevail from 0.25 height strain onwards, where retardation in the stress raise can also be observed as compared to the initial stage. This is due to the dislocation of internal particles along with pores in both axial and radial directions. It is reported that in the second stage, dislocation is more in radial than in the axial direction as the particle movement in axial direction contributes to the matrix hardening and subsequently stress raise [7]. It is noted that P/M material under plastic deformation exposed not only to matrix hardening as well as to geometric hardening this is due to the closure of porosities. Further, it is noticed that smaller the aspect ratio and higher the friction condition, enhances the resistance to deformation substantially. The Fe of 0.3 and 0.6 aspect ratio deformed under nil lubricant shows higher stress values for any given height strain as compared to the same preforms deformed under graphite lubricant. Since, higher friction condition hinders the dislocation of particles in radial direction that lead to higher resistance to deformation. With regards to the influence of aspect ratios, it was observed that Fe of 0.3 aspect ratios deformed irrespective of friction conditions show higher stress values as compared to 0.6 aspect ratio preforms. As the smaller aspect ratio preforms undergo more uniform load distribution that enhances the resistance to deformation at much faster rate. Almost similar characteristics observations were found for Fe-0.4%C preforms as far as the influence of aspect ratios and lubricants concerned. On the side of the influence of compositions for two different aspect ratios it can be observed that the Fe-0.4%C steel preforms show bit higher stress values than Fe preforms on the later stage of deformation as compared to the initial stage of deformation. Another careful observation reveals that dispersion of curves between the compositions is much evident in nil lubricant rather than in the graphite lubricant condition.

The true stress against true strain is plotted on log-log graph in order to predict strain hardening parameters which is shown in Figure 3.

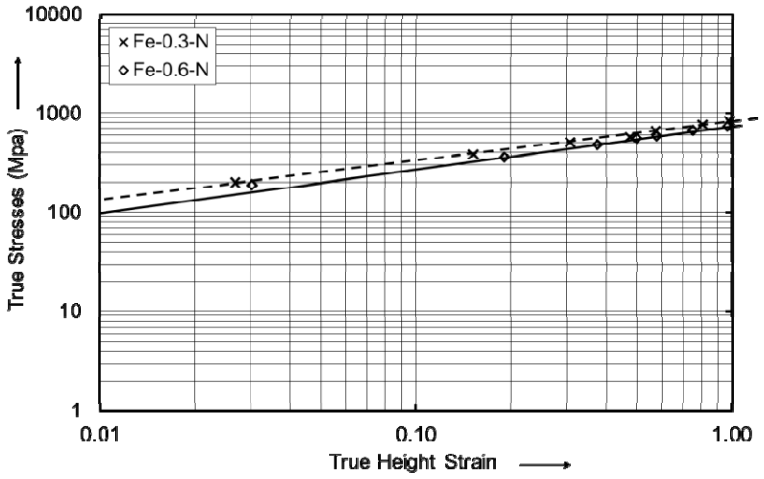

Figure 3. Stress-strain in log-log plot.

Figure 3 is shown for iron preforms that are deformed under nil lubricant but with two different aspect ratios. It reveals that increase of height strain is proportionately improves the stress, however, 0.3 aspect ratio preform resists deformation at higher pace than 0.6 aspect ratio preform. The similar observation has been made in Figure 2 as well. A power law relationship can be drawn from Figure 3, for stress-strain that follows the Ludwik's strain hardening equation as:

$$\sigma = K\varepsilon^n \tag{2}$$

where σ is true stress and ε is true strain, the K is strength coefficient and n is the strain hardening parameter. The K and n are determined by finding the intercept and slope in Figure 3, respectively. Similarly plots were made for all other combinations of variables in order to predict their respective K and n values. The predicted values are shown in Table 2.

7. Formulation of mathematical models and estimation of factor effects

7.1. General regression model

The general regression model shall be formulated in the following form for K and n:

$$K = \alpha_0 + \alpha_1 C + \alpha_2 A + \alpha_3 CA + \alpha_4 L + \alpha_5 CL + \alpha_6 AL + \alpha_7 CAL \tag{3}$$

$$n = \beta_0 + \beta_1 C + \beta_2 A + \beta_3 CA + \beta_4 L + \beta_5 CL + \beta_6 AL + \beta_7 CAL \tag{4}$$

where, α_0 through α_7 and β_0 through β_7 are coefficients of main factor effects and interaction factor effects for K and n respectively.

7.2. Yate's algorithm

The $K \; or \; n = f(C, A, L)$; The models (3) and (4) include all the main factors and its first order interactions. The estimation of main factor and its interaction effects are calculated using Yate's algorithm. The results are shown in Table 4.

Table 4. Estimation of main and interaction factor effects for *K*.

Factor	Response K in MPa		Total	Yates Column			Factor	Sum of	Co-eff. of regression
order	Trial 1	Trial 2	Response	(1)	(2)	(3)	estimate	Squares (SS)	model (CF)
[1]	125	120	245				198.00	156816.00	99
C	120	112	232	375	732	−18	−2.25	20.25	−1.125
A	99	90	189	400	−16	−170	−21.25	1806.25	−10.625
CA	96	90	186	332	−2	12	1.50	9.00	0.75
L	91	110	201	−13	−102	−120	−15.00	900.00	−7.5
CL	100	99	199	−3	−68	14	1.75	12.25	0.875
AL	76	90	166	−2	10	34	4.25	72.25	2.125
CAL	87	79	166	0	2	−8	−1.00	4.00	−0.5

In addition to the estimation of "factor effects", the sum of squares and the coefficients for the mathematical model are also calculated and portrayed in Table 4.

$$SS = \frac{Yates\ column\ (3)^2}{2n^*} \tag{5}$$

$$CF = \frac{SS}{Yates\ column\ (3)} \tag{6}$$

where, n^* is total number of experimental orders, the Yate's algorithm and its corresponding column (1), (2) and (3) predictions are explained elsewhere [17]. It can further be noted that the *CF* shall be determined from the factor estimate as well.

7.3. ANOVA study

The main and interaction factors estimated from Yate's algorithm should be validated to understand which factors are most influential and less or no influential, accordingly the model shall be refined. Thus ANOVA study is implemented to carry out; for which a R-software is used [18,19], whose results for strength coefficient, *K* are tabulated in Table 5.

Table 5. ANOVA for *K*.

Source of variation	Sum of Squares	Degrees of freedom	Mean square	$F_{calculated}$	$F_{critical}$	% contribution
C	20.25	1	20.25	0.3913	0.54904	0.63
A	1806.25	1	1806.25	34.9034	0.00036	55.78
CA	9	1	9	0.1739	0.68762	0.28
L	900	1	900	17.3913	0.00312	27.79
CL	12.25	1	12.25	0.2367	0.63964	0.38
AL	72.25	1	72.25	1.3961	0.2713	2.23
CAL	4	1	4	0.0773	0.78805	0.12
Residuals	414	8	51.75			12.79
Total	3238	15				

Faraway described in detail with explanations the terms and the expressions for sum of squares, degrees of freedom and mean squares [20]. The % contribution by each factors were also included in Table 5. The expression used to calculate for percentage contribution is:

$$\%\ Contribution = \frac{Sum\ of\ squares}{Total\ sum\ of\ squares} \times 100 \tag{7}$$

It can be observed from the table that maximum contribution is made by aspect ratios, then lubricants followed by the interaction of aspect ratios and lubricants. It is important to note that the main factor composition and the interaction of compositions, aspect ratios and lubricants together as well as interaction of lubricants and aspect ratios individually with composition makes negligible contribution. The same phenomenon can also be proved by observing the values of F calculated, F_{cal}, and F critical values, F_{crit}, in Table 5. The F_{crit} value can either be obtained from F distribution table for 95% confidence level or these values shall be predicted by the R-software itself. The F_{cal} shall be determined using mean square value divided by mean square residual. Now comparing the value of F_{cal} and F_{crit}, the necessary conclusion shall be drawn. For instance, if, $F_{cal} > F_{crit}$, indicates the corresponding factor making significant effect; else, $F_{cal} \leq F_{crit}$ indicates the factor makes no significant effect on strain hardening characteristics.

8. Regression model

The generic model for K was given in Eq 3. The coefficients are found in Table 4 that can be substituted in Eq 3 as follows:

$$K = 99 - 1.125C - 10.625A + 0.75CA - 7.5L + 0.875CL + 2.125AL - 0.5CAL \tag{8}$$

The significant factors that contributes for the influence of strength coefficient is studied using ANOVA in Table 5, thus Eq 8 can be refined into the following form:

$$K = 99 - 1.125C - 10.625A - 7.5L + 2.125AL \tag{9}$$

Similarly the final expression for, n has been formulated as follows:

$$n = 0.4388 + 0.015A + 0.01L + 0.00625CAL \tag{10}$$

It can be noted from Eq 10 that for "n", aspect ratios, A, and lubricants, L, making significant effect, further interaction factor, CAL also making significant effect; unlike it was observed in Eq 8, where CAL makes no effect in "K".

9. Residual analysis and model adequacy

The residuals or error for the model, Eq 9 is found using the following expression:

$$Residual = K_o - K_p \tag{11}$$

where, K_o is strength coefficient observed or found from experiments and K_p is strength coefficient predicted using model, Eq 9.

To express the residual analysis, the plot for residual against K_p, normal score and normal probability is drawn and it is shown in Figures 4, 5 and 6 respectively. Similar plots for "n" are shown in Figures 7, 8 and 9, respectively.

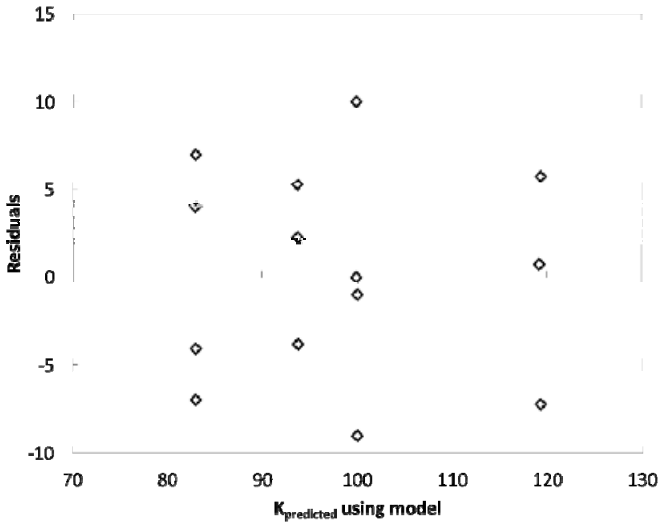

Figure 4. Residual against K_p.

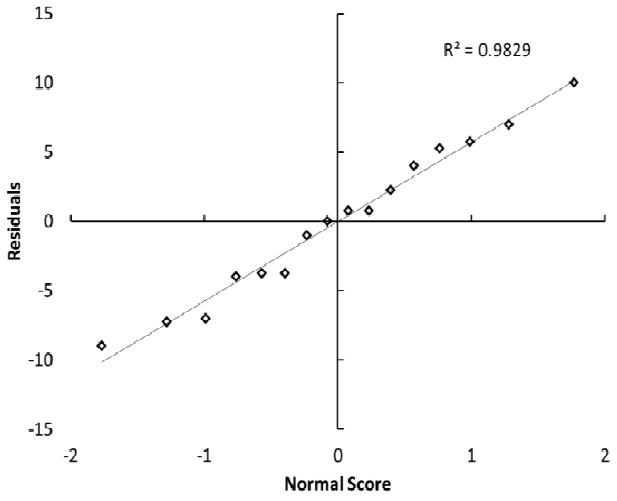

Figure 5. Residuals vs normal score for K.

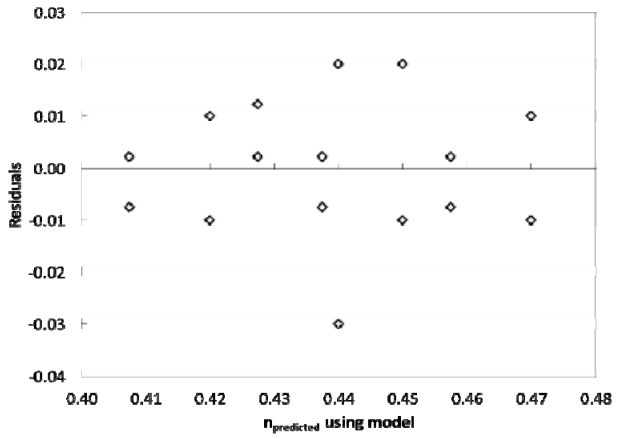

Figure 6. Residual vs normal probability for *K*.

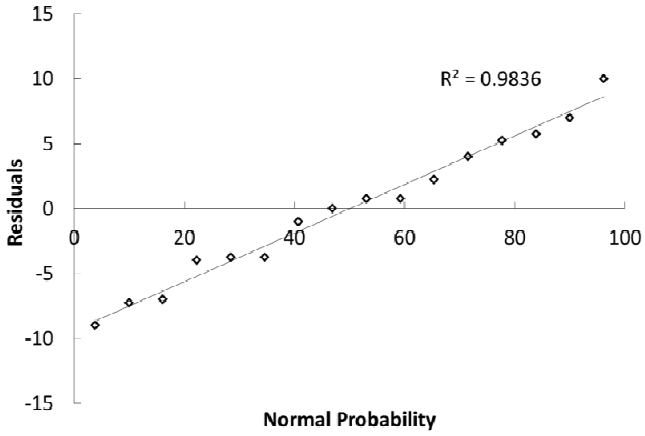

Figure 7. Residual vs predicted *n*.

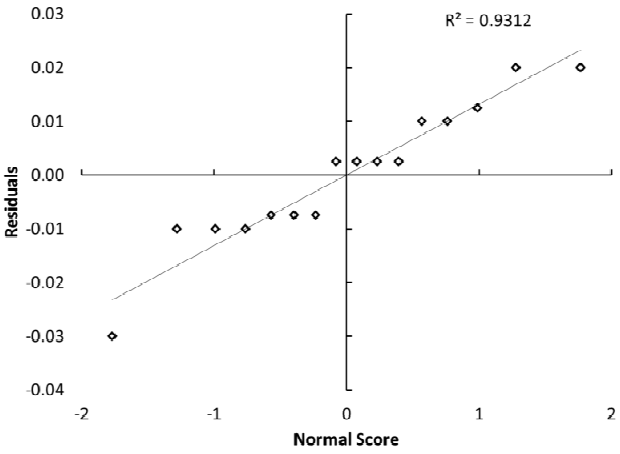

Figure 8. Residuals vs normal score for *n*.

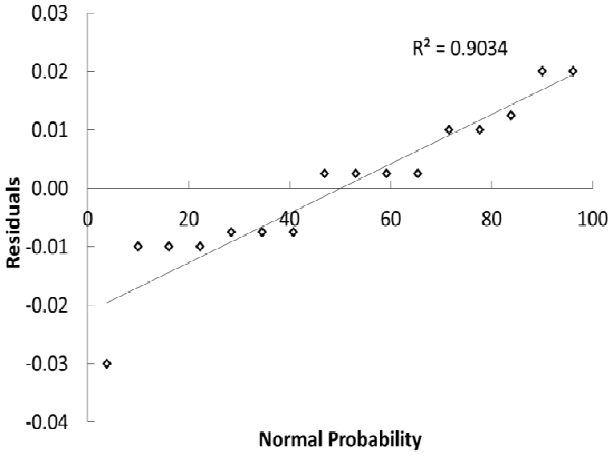

Figure 9. Residual vs normal probability for *n*.

It can be observed from Figure 4, that residuals mostly fall in ±5 except few residuals that falls apart; however the correlation coefficient predicted for residuals against normal score and normal probability is 0.98. This confirms that the residuals or well within the control limit. A similar observation can be made for "n" from Figures 7 through 9, whose residuals correlation coefficient is found to be 0.93 maximum. Further an attempt has been made to cross check the adequacy of model using regression coefficient, *r*, which is also found to follow 0.9, such as 0.93 for *K* and 0.9 for *n*. The expression to determine, *r*, is as follows [21].

$$r = \sqrt{\frac{\sum(K_p - \overline{K}_o)^2}{\sum(K_o - \overline{K}_o)^2}} \tag{12}$$

where, $\overline{K}_o$, is the average of K_o values.

10. Results and discussion

The mathematical model developed in the present investigation is proven to follow much close tolerance to the observed values, thus the model can be used to predict strain hardening characteristics values for the chosen variables of interest with the specified levels. The data generated from the models are plotted as response surface and contour plot for *K*, which is shown in Figures 10 and 11 respectively. A similar plot was drawn for *n* and is shown in Figures 12 and 13, respectively.

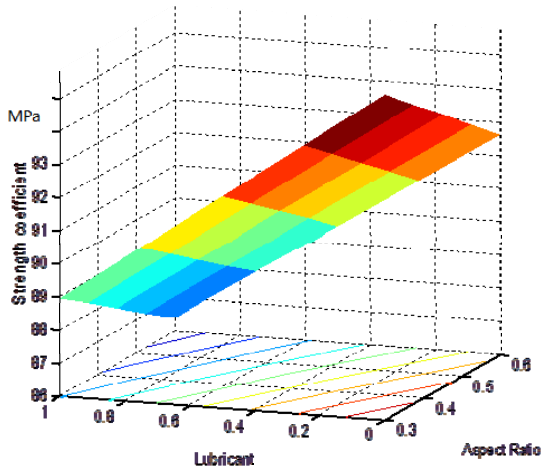

Figure 10. Response surface plot for *K*.

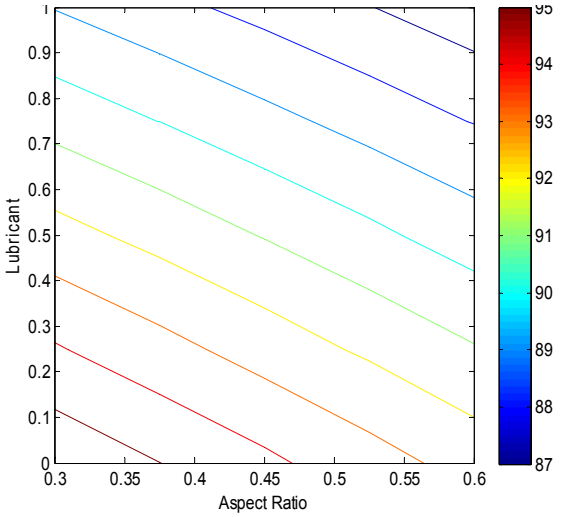

Figure 11. Contour plot for *K*.

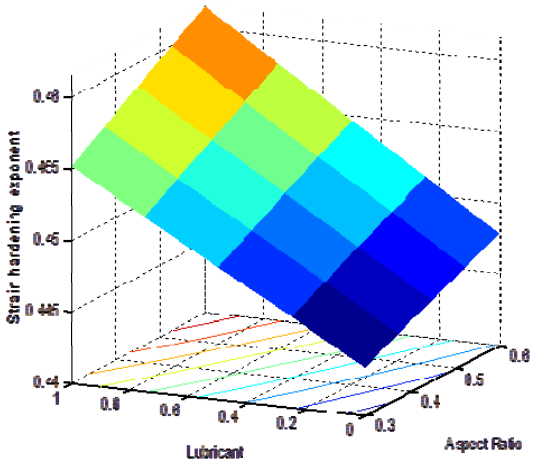

Figure 12. Response surface plot for *n*.

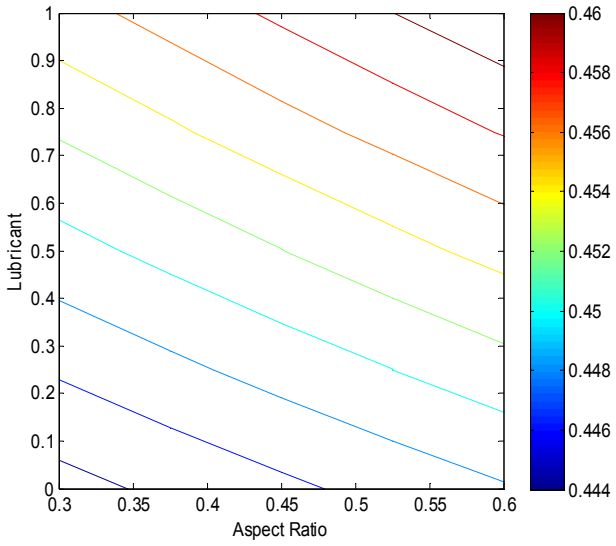

Figure 13. Contour plot for *n*.

It is noted from Figures 10 and 11 that the influence of aspect ratios is bit greater than the influence of lubricants. Further it can be observed that decreasing the aspect ratio along with decreasing the lubricant substantially improves the strength coefficient. The contour and response surface plot can be utilised to design the components for the required strength coefficient, *K*. For instance to obtain *K* value of 93 MPa and above, the aspect ratio of less than or equal to 0.55 with lubricant value of 0 to 0.4 should be chosen. Thus the plots can be used as a tool to identify the parameters range in order to obtain a particular strain hardening characteristics.

Similarly, response surface and contour plot (Figures 12 and 13) for *n*, reveals that decreasing lubricant and decreasing aspect ratio leads to less strain hardening exponent. On the other hand increasing both the parameters leads to highest, *n*, value. It is also important to note from the contour plot (Figure 13) the lines are bit curved, which is due to the interaction effect of the compositions.

11. Conclusions

The following are the major findings from the present investigation:

- The mathematical model for strain hardening characteristics of Fe and Fe-0.4%C with the influence of aspect ratios and lubricants are developed. The values predicted through models are found to have close tolerance with the experimentally observed values. Therefore for the chosen limits of the influencing variables this model can directly be utilised to predict strain hardening parameters. By this unnecessarily performing experiments can be avoided apart from saving time and materials.
- The surface response and contour plot developed using the mathematical model shall be utilised as a tool to identify the parameters range in order to obtain a particular strain hardening characteristics. For instance to produce components with the strength coefficient of 93 MPa or above, the aspect ratio of ≤0.55 and the lubricant of ≤0.4 can be chosen.
- The addition of 0.4%C with Fe show nil influence in strength coefficient, *K*, however little influence is evident for strain hardening exponent, *n*. On the other hand, decreasing aspect ratios and the lubricants substantially improves strength *K* but retards *n*.

Conflict of interest

The authors declare no conflict of interest.

References

1. Rajeshkannan A, Narayan S (2009) Strain hardening behaviour in sintered Fe-0.8%C-1.0%Si-0.8%Cu powder metallurgy preform during cold upsetting. *J Eng Manuf* 223: 1567–1574.
2. Kaku SMY, Khanra AK, Davidson MJ (2018) Effect of deformation on properties of Al/Al-alloy ZrB_2 powder metallurgy composite. *J Alloy Comp* 747: 666–675.
3. Taub AI, Babu SS (2018) Opportunities and challenges for introducing new lightweight metals in transportation. *Int J Powder Metall* 54: 27–33.
4. Mascarenhas J (2004) Powder metallurgy: A major partner of sustainable development. *Mater Sci Forum* 455: 857–860.
5. Straffelini G (2005) Strain hardening behaviour of powder metallurgy alloys. *Powder Metall* 48: 189–192.
6. Luo J, Li M, Yu W, et al. (2010) The variation of strain rate sensitivity exponent and strain hardening exponent in isothermal compression of Ti-6Al-4V alloy. *Mater Des* 31: 741–748.
7. Narayan S, Rajeshkannan A (2011) Strain hardening behaviour in forming of sintered iron-0.35% carbon powder metallurgy preform during cold upsetting. *Mater Res* 14: 1–7.
8. Ebrahimi R, Pardis N (2009) Determination of strain-hardening exponent using double compression test. *Mater Sci Eng A* 518: 56–60.
9. Bouaziz O, Zurob H, Chehab B, et al. (2011) Effect of chemical composition on work hardening of Fe-Mn-C TWIP steels. *Mater Sci Tech* 27: 707–709.
10. Narayan S, Rajeshkannan A (2011) Influence of carbon content on strain hardening behaviour of sintered plain carbon steel preforms. *J Iron Steel Res Int* 18: 33–40.
11. Zhang X, Zhang Y, Du S, et al. (2018) Study on the tribological performance of copper based powder metallurgical friction materials with Cu coated or uncoated graphite particles as lubricants. *Mater* 11: 1–18.
12. Rajeshkannan A, Narayan S (2013) Phenomenon of instantaneous work hardening characteristics of sintered cold deformed Cu alloy preforms. *Adv Mater Res* 651: 295–301.
13. Selvakumar N, Narayanasamy R, Pandey KS (2004) Some aspects of cold upset forming of sintered aluminum preforms using different lubricants. *Powder Metall Metal Ceramics* 43: 349–354.
14. Li W, Park SJ, Suri P, et al. (2009) Investigation on die wear behaviour during compaction of aluminium matrix composite powders. *Powder Metall* 54: 202–208.
15. Narayanasamy R, Anandakrishnan V, Pandey KS (2008) Comparison of workability strain and stress parameters of powder metallurgy steels AISI 9840 and AISI 9845 during cold upsetting. *Mater Des* 29: 1919–1925.
16. Linda MC, John JD, Runze L (2009) Design of experiments with multiple independent variables: a resource management perspective on complete and reduced factorial designs. *Psychol Methods* 14: 202–224.

17. Krishnamurthy L, Sridhara BK, Budan DA (2007) Comparative study on the machinability aspects of aluminium silicon carbide and aluminium graphite composites. *Mater Manuf Process* 22: 903–908.
18. R core team (2013) R: A language and environment for statistical computing. R foundation for statistical computing, Vienna, Austria. Available from: http://www.R-project.org/.
19. Regti A, Laamari MR, Stiriba SE, et al. (2017) Use of response factorial design for process optimization of basic dye adsorption onto activated carbon derived from Persea species. *Microchem J* 130: 129–136.
20. Faraway JJ (2002) Practical Regression and Anova Using R. 1st ed. University of Bath, 168.
21. Douglas CM (2017) Design and analysis of experiments, 9th ed., Wiley Publisher, New Jersey, 238–253.

AIMS Press